Materials Science Forum
ISSN: 1662-9752, Vol. 1146, pp 3-11
doi:10.4028/p-gA8WDg

Submitted: 2024-05-21
Revised: 2024-07-29
Accepted: 2024-10-01
Online: 2025-03-18

Powder Metallurgy and Heat Treatment Effects on Microstructure in a γ-TiAl Ti-4522XD Alloy

B. Ruiz–Palenzuela[1,2,a], I. Sabirov[3,b] and E. M. Ruiz–Navas[1,c]

[1]Departament of Materials, Universidad Carlos III de Madrid, Legane´s, Spain

[2]European Organization for Nuclear Research, Geneva, Switzerland

[3]IMDEA Materials Institute, Getafe, Madrid, Spain

[a]berta.ruiz.palenzuela@cern.ch, [b]ilchat.sabirov@imdea.org, [c]emruiz@ing.uc3m.es

Keywords: γ-TiAl, Powder Metallurgy, Microstructure, Intermetallics, Thermal Treatments

Abstract. This investigation focuses on the microstructural refinement of the *γ*-TiAl intermetallic alloy Ti-45Al-2Nb-2Mn (at.%) + 0.8 (vol.%) TiB_2 (Ti4522XD) processed by powder metallurgy. The alloy powders were manufactured using the Electrode Induction-melting Gas Atomization (EIGA) process and subsequently consolidated through Hot Isostatic Pressing (HIP), resulting in a near-*γ* microstructure.

The study further explores the effects of three distinct thermal treatments on the microstructure: 1) heating to 1300˚C for 2 hours followed by furnace cooling (HT1), 2) heating to 1300˚C for 2 hours, then water quenching and aging at 850˚C for 8 hours before furnace cooling (HT2), and 3) heating to 1300˚C for 2 hours, followed by water quenching and aging at 700˚C for 8 hours before furnace cooling (HT3). These processes were tailored to promote the development of duplex (DP) and fully lamellar (FL) microstructures.

Characterization was performed using X-ray diffraction (XRD) to identify phase distributions and scanning electron microscopy (SEM) to examine the surface morphology. Transmission electron microscopy (TEM) was used for a preliminary assessment of actual lamellar spacing. As a result, two different microstructures were obtained: DP for HT1 and near fully lamellar (NFL) for HT2 and HT3, but differences in the final actual lamellar spacing were observed for these last two cases. Additionally, the presence of microcracks of different morphologies was observed by SEM prior to any mechanical testing.

1 Introduction

Titanium aluminides, particularly gamma titanium aluminides (*γ*-TiAl), represent a significant advancement in intermetallic materials, combining low density with high-temperature resistance. These properties make *γ*-TiAl alloys attractive for aerospace and automotive applications, where reducing weight while maintaining strength is crucial. Furthermore, their resistance to oxidation at high temperatures positions these alloys as viable alternatives to heavier nickel-based superalloys [1–4].

Traditionally, the production of *γ*-TiAl alloys has been carried out through conventional ingot metallurgy as well as investment casting. However, heterogeneous microstructures have been observed as a consequence of segregation in the case of large pieces using these techniques, due to slow solidification. This leads to the necessity of subsequent steps to arrive at the final state [5–7]. As a result, powder metallurgy has emerged as a powerful candidate because it enhances microstructural refinement and offers higher reproducibility and homogeneity, along with a substantial decrease in the necessary processing steps [2, 8–10]. For the production of the powders, EIGA is preferred for these materials due to its ability to produce powders with low oxygen content and uniform alloy composition, which are essential for achieving the desired properties in the final product [6]. Following powder production, Hot Isostatic Pressing (HIP) was utilized to consolidate the powders into solid components. HIP helps in eliminating porosity, thus enhancing the mechanical properties of the alloys [11].

Microstructural control is pivotal in determining the mechanical behavior of γ-TiAl alloys. These alloys can exhibit various microstructures, such as fully lamellar, duplex, and near-gamma, each of which provides distinct mechanical advantages. The fully lamellar structure, for instance, offers excellent creep resistance, making it suitable for high-temperature applications, while the duplex structure provides a balance of ductility and strength [2, 12]. However, it has been observed that factors such as lamellar spacing and lamellar colony size significantly impact mechanical performance [10, 13].

2 Materials and Experimental Procedures

2.1 Material and Processing. For this study, the TiAl alloy Ti-45Al-2Nb-2Mn (at.%) with 0.8 (vol.%) TiB_2, referred to as Ti4522XD, was utilized. This specific formulation was processed from atomized prealloyed powder via EIGA, followed by sintering under HIP at 1200˚C for 4 hours under 200 MPa pressure [6].

Specimens for analysis were shaped into cylinders, 10 mm in diameter and 15 mm in length, to meet the dimensional requirements for further testing. Encased in glass capsules (Fig.1) under a vacuum to prevent oxidation, these specimens underwent a series of carefully controlled thermal treatments. These treatments are divided into four distinct stages: solubilization, first cooling, stabilization, and second cooling, as outlined in Tab. 1.

The initial solubilization stage involves heating to 1300˚C, surpassing the T_α temperature, a step found to be essential for inducing fully lamellar microstructures [14]. However, the necessity to increase the temperature above T_α is reported to be highly sensitive to the precise alloy composition, such as slight variations in Al content [15], as well as to the presence of impurities like O, C, H, and N [16].

Table 1. Heat treatments stages and codification

Codification	Treatment Stages
HT1	1300ºC/2h/FC
Intermediate microstructure	1300ºC/2h/WQ
HT2	1300ºC/2h/WQ + 850˚C/8h/FC
HT3	1300ºC/2h/WQ + 700˚C/8h/FC

Fig. 1. Samples inside glass encapsulation with vacuum atmosphere inside

According to Novoselova et al. [17], crucial microstructural parameters, such as lamellar colony size and lamellar spacing, are significantly influenced by the specifics of the heat treatment—namely temperature, holding time, and cooling rate. These parameters are so critical that some authors have reported the potential for coarsening of lamellar spacing within just minutes of hold time at temperatures exceeding T_α [5, 8, 18, 19]. Furthermore, alternative strategies have been proposed to counteract this effect. For instance, the addition of boron and an increase in the temperature during the solubilization stage, to reach the $\alpha + \beta$ phase field, can inhibit the growth of α grains due to the presence of β grains [12, 17]. In this specific case, the stabilization temperature was maintained close to T_α (see Fig.2), with the same holding time for all cases, to minimize the variety in microstructure. Additionally, the goal was to reduce the temperature for this stage to enhance processing economics and cost-effectiveness.

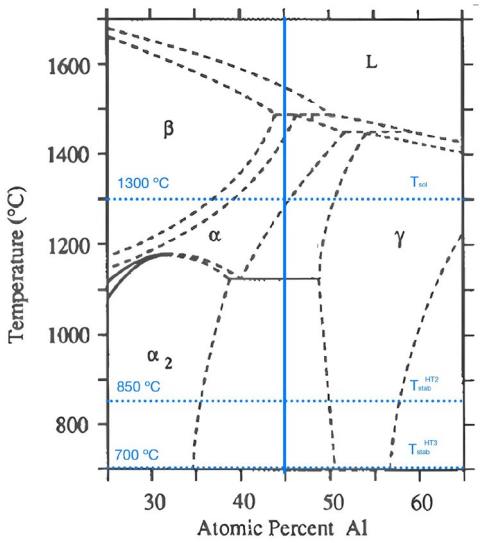

Fig. 2. Superposition of the temperatures for the different heat treatments conducted in this study over the phase diagram of TiAl, focusing on the area of interest of the composition studied herein. Here, T_{sol} stands for the solubilization temperature, and T_{stab} stands for the stabilization temperature [14].

The subsequent cooling stage varied; HT1 specimens underwent furnace cooling (FC) to develop a duplex microstructure, contrasting with the rapid water quenching (WQ) applied to HT2 and HT3 treatments designed to foster lamellar structures [5]. For treatments other than HT1, a stabilization stage at two different temperatures followed [6], extending for 8 hours to evaluate the effects on lamella thickening [16]. A final furnace cooling concluded the thermal treatment process for all three cases. Notably, specimens submitted to water quenching required re-encapsulation due to the breakage of the capsule during the cooling, ensuring the integrity of the inert atmosphere of the subsequent stabilization stage.

2.2 Microstructural Characterization. The microstructures resulting from the previously described thermal treatments were characterized using XRD, SEM, and TEM. XRD experiments were performed on an Empyrean PANalytical diffractometer equipped with a Cu-Kα source, operating at 45 kV and 40 mA. A 2θ-range of 15–80° was scanned with a step size of 0.02° and a dwell time of approximately 150 s. To investigate the relationship between microstructure and the presence and propagation of cracks, specimens were observed by SEM. SEM analyses were conducted with an EVA MA 15 machine equipped with a backscattered (BSE) electron detector and operated at 20 kV. Due to its higher resolution, a field emission gun scanning electron microscope (FEG-SEM) Helios Nanolab 600i was also utilized for the analysis of samples, owing to the small size of the observed microstructural features. Samples for microstructural characterization were prepared using standard metallographic techniques, with OP-S polishing to achieve a mirror-like surface at the final stage. For all SEM images reported herein, areas with a darker contrast correspond to the γ phase, while areas with brighter contrast correspond to the α_2 phase, and whitish particles are identified as TiB_2 particles.

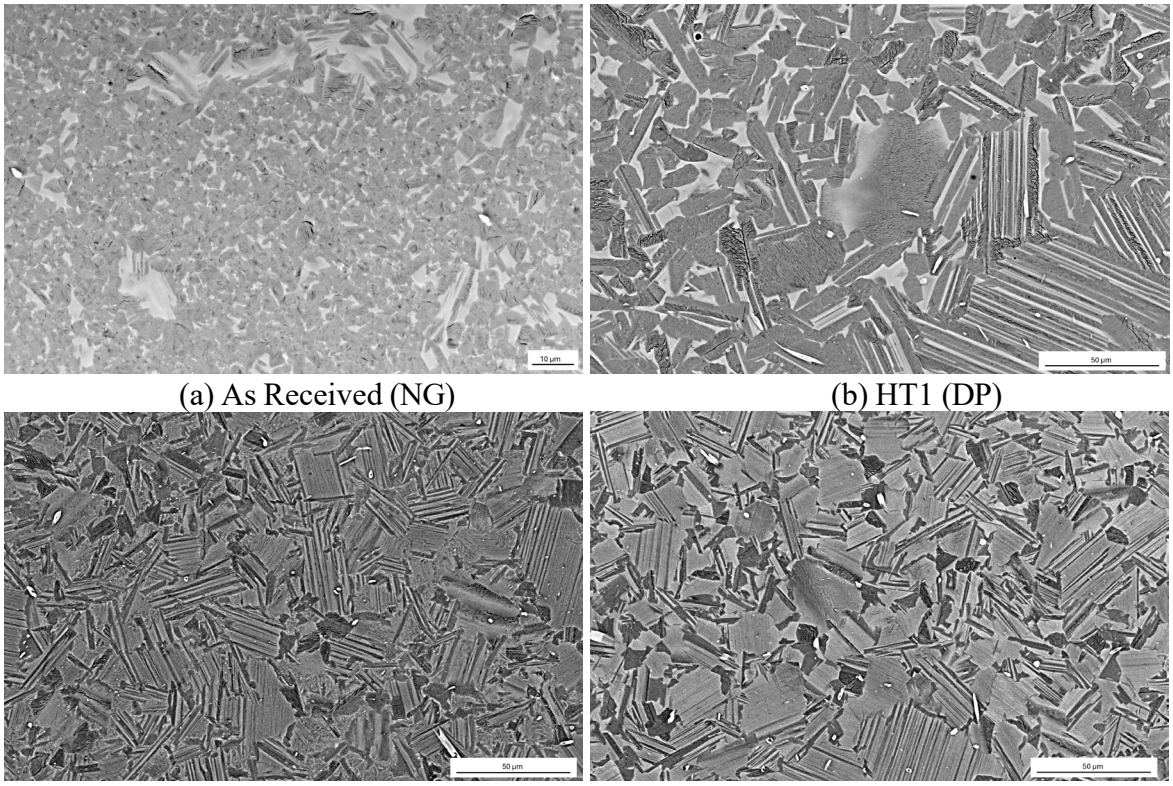

(a) As Received (NG) (b) HT1 (DP)

(c) HT2 (NFL) (d) HT3 (NFL)

Fig. 3. SEM (BSE) images showing the microstructures of samples in various states.

TEM studies were carried out in bright-field (BF) and high-angle annular dark field (HAADF) modes with a FEG S/TEM (Talos F200X, FEI) operated at an accelerating voltage of 200 kV. The resulting TEM images were used to estimate the lamellar spacings of the microstructures. For TEM specimen preparation, specimens were mechanically ground to a thickness of approximately 100 µm, followed by electropolishing at −30 ˚C, 40 V, for 10 s using an electrolyte consisting of 60 % methanol, 34 % butoxyethanol, and 6 % perchloric acid (vol %). The process was carried out in a twin-jet electropolishing equipment (TenuPol 5, Struers®).

3 Results and Discussion

3.1 Effect of Heat Treatment on Microstructure. The microstructure resulting from powder metallurgy consolidation (EIGA and HIP) exhibited a NG microstructure, as depicted in Fig. 3a. In this figure, a predominant amount of γ grains are enclosed within a lesser α_2 matrix. No porosity was detected; however, cracks were noted within the γ grains and at the interfaces between the γ and α_2 phases. XRD phase analysis corroborated this observation, indicating a predominance of the γ phase. After the execution of the heat treatments, the material underwent distinct microstructural transformations. Specimens treated with HT1 (Fig. 3b) displayed a significant shift to a DP microstructure, with both γ grains and lamellar colonies evident. XRD confirmed these findings by revealing an enhanced α_2 phase presence alongside the dominant γ phase, indicating a balanced development of
these components.

For the specimens subjected to HT2 and HT3 treatments (Figs. 3c and 3d, respectively), the outcomes showed distinct variations. Both sets of samples predominantly exhibited a NFL microstructure, characterized by an increase in lamellar colonies interspersed with some γ grains. XRD analysis revealed a more pronounced shift towards NFL structures in the HT2 samples, with the α_2 phase being more prominent. In contrast, HT3 samples exhibited a greater presence of the γ phase, accompanied by a slightly reduced actual lamellar spacing, and the lamellar colonies appeared to be smaller.

Additionally, an incipient globulization was observed in several areas of some HT2 specimens as can be observed in Fig. 4c.
An intermediate microstructure (Intermediate microstructure as defined in Tab. 1) was examined, revealing a substantial increase in lamellar colony size (Fig. 4a), with γ grains appearing only marginally. This confirms that the addition of a stabilization stage promote thickening and coarsening of the γ lamellae, as well as existing γ grains, potentially leading to microstructures akin to those observed in HT2 and HT3 samples. In this stage, no evidence of the globulization process was detected, highlighting its absence during the early phases of cooling.

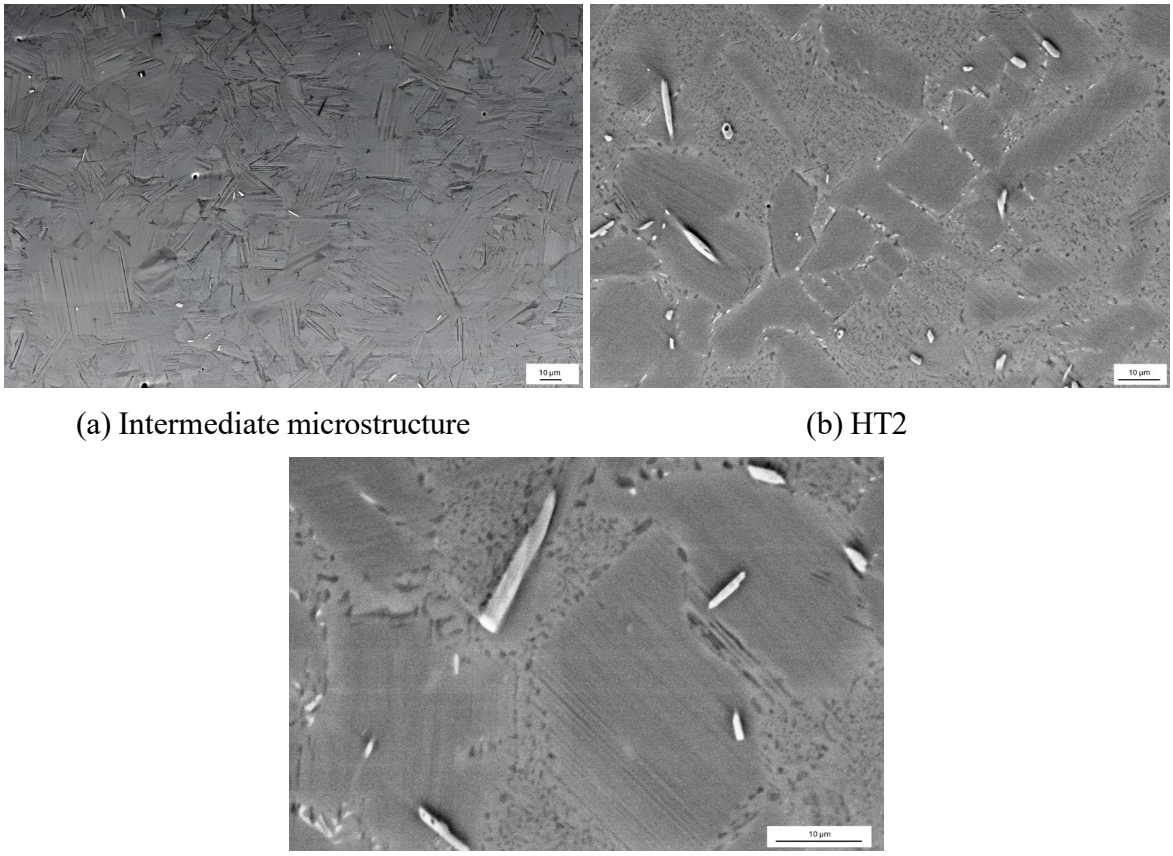

(a) Intermediate microstructure (b) HT2

(c) HT2 higher magnification

Fig. 4. SEM (BSE) images showing the intermediate microstructure and HT2 specimens, which present globulization.

Lastly, the presence of TiB_2 particles was noted in all cases. However, in HT1 and the as-received material, these particles were observed to be smaller and more evenly distributed, while samples from HT2 and HT3 treatments exhibited larger, more acicular TiB_2 particles, though in fewer numbers.
Specimens from HT2, where globulization was observed, showed an actual increase in the number and length of TiB_2 particles, giving them a more acicular appearance. Due to the limited quantity of TiB_2 particles, they were not detectable by XRD, and thus no peaks were assignable in the XRD spectra (Fig. 5).

3.1.1 Presence of Microcracks. Microcracks were detected in all DP and NFL microstructures, irrespective of the treatment applied, as well as in the initial NG microstructure. These cracks were primarily found in areas with darker contrast, which, according to Energy Dispersive Spectroscopy (EDS) analysis, correlates with the γ phase. The consistent emergence of microcracks, particularly in regions associated with the γ phase, highlights the potential mechanical implications of phase distribution within the alloy as well as the residual stresses resulting from the thermal treatments and the reduced ductility attributed to the γ grains [2, 10, 20]. Moreover, these microcracks were also observed within lamellar colonies, affecting those identified with the contrast corresponding to the γ phase.

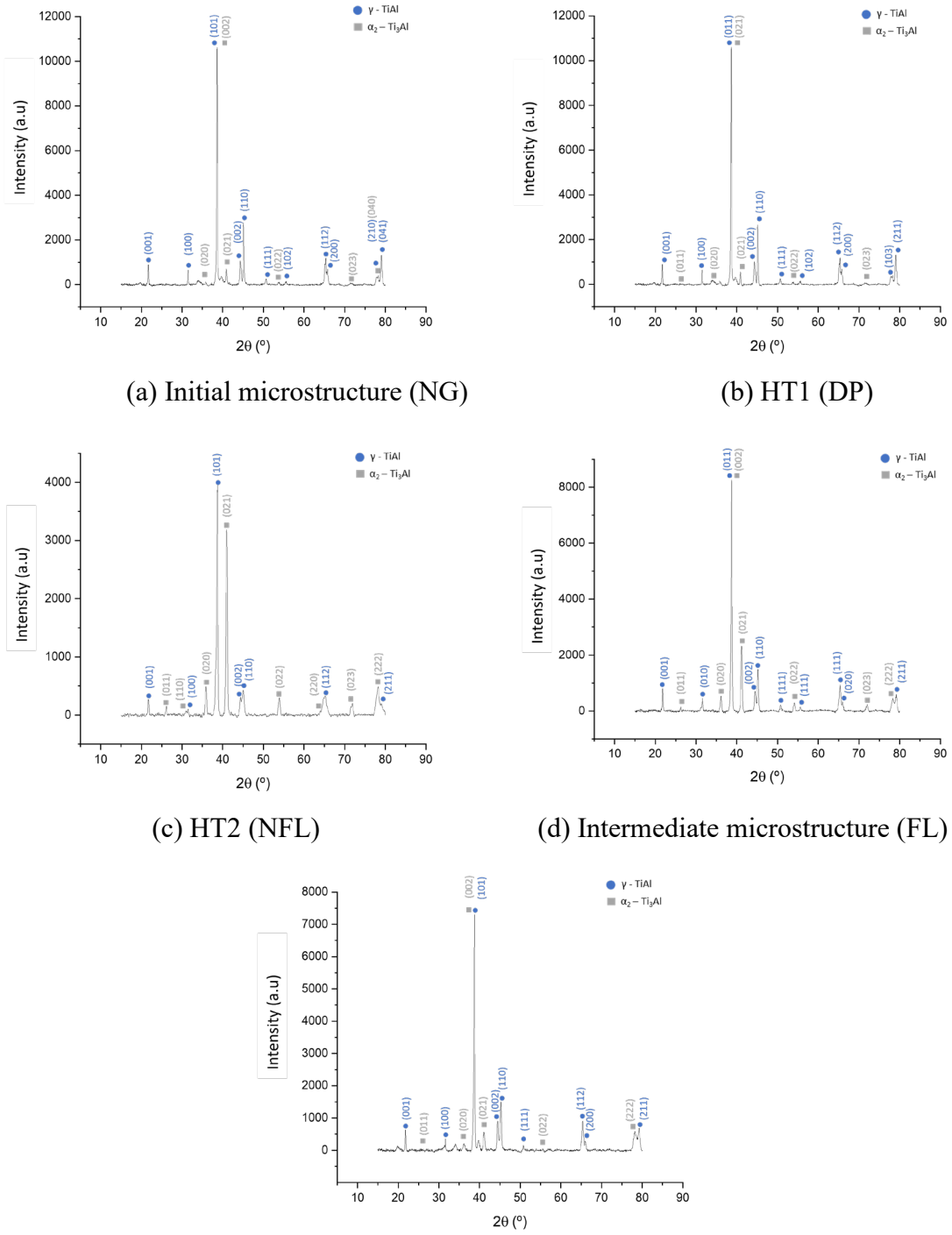

(a) Initial microstructure (NG)

(b) HT1 (DP)

(c) HT2 (NFL)

(d) Intermediate microstructure (FL)

(e) HT3 (NFL)

Fig.5. XRD spectra for the various microstructures. Peaks are identified for the γ and α_2 phases.

Both interlamellar and intralamellar microcrack morphologies, as observed in Fig. 6, were found across the colonies, regardless of whether DP or NFL microstructures were examined. However, no such observations were made for specimens exhibiting signs of globulization. Slight differences were noted between HT2 and HT3; notably, HT3 samples exhibited fewer detectable microcracks within the lamellar colonies, likely due to the reduced actual lamellar spacing.

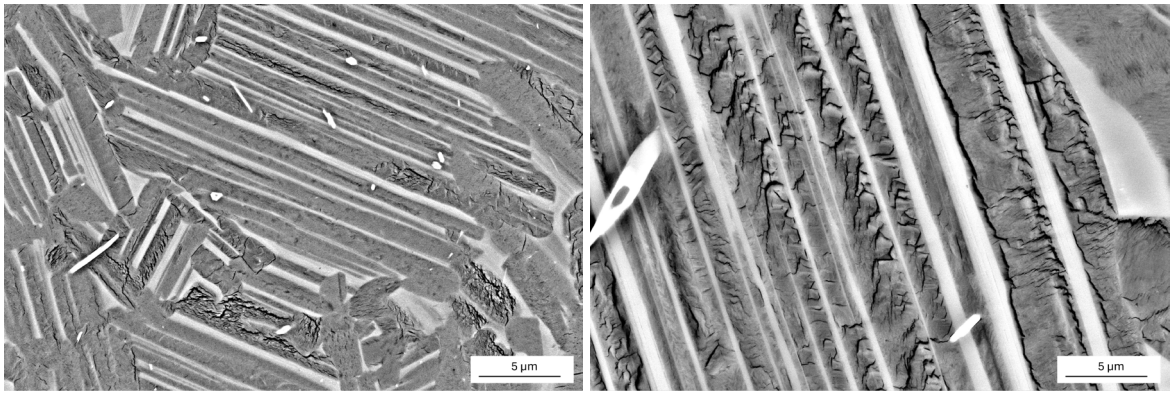

(a) HT1 (b) HT1 detail in lamellar colony

Fig. 6. SEM (BSE) images showing microcracks observed in the different herein reported microstructures.

3.1.2 Actual Lamellar Spacing Assessment. However, significant challenges are encountered when analysis is attempted via SEM in accurately assessing the real lamellar spacing, as illustrated in Fig. 7, where inner lamellae of similar contrast were found within an area previously categorized as a single lamella. These observations highlight the small size of these features being in the nanometer range.

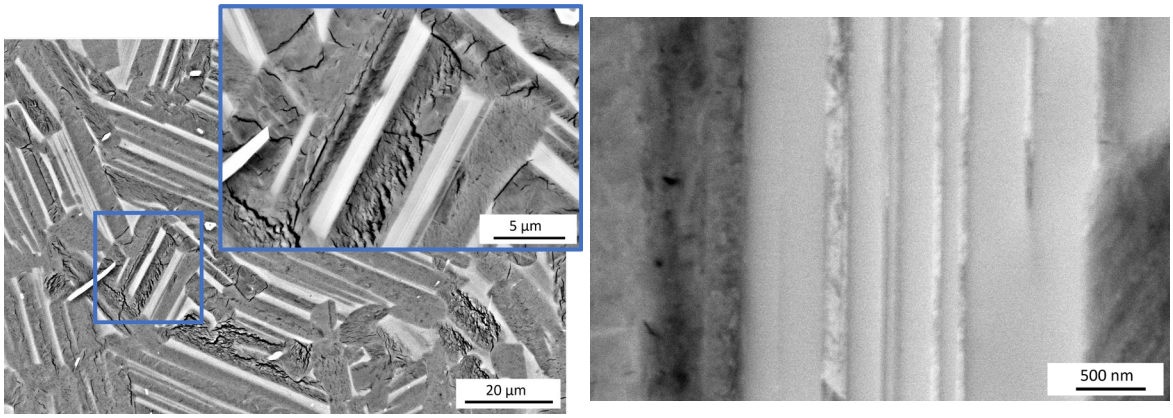

Fig. 7. SEM (BSE) images showing an example of inner lamellar structures within lamellae of the same contrast. High magnification of the area on the right.

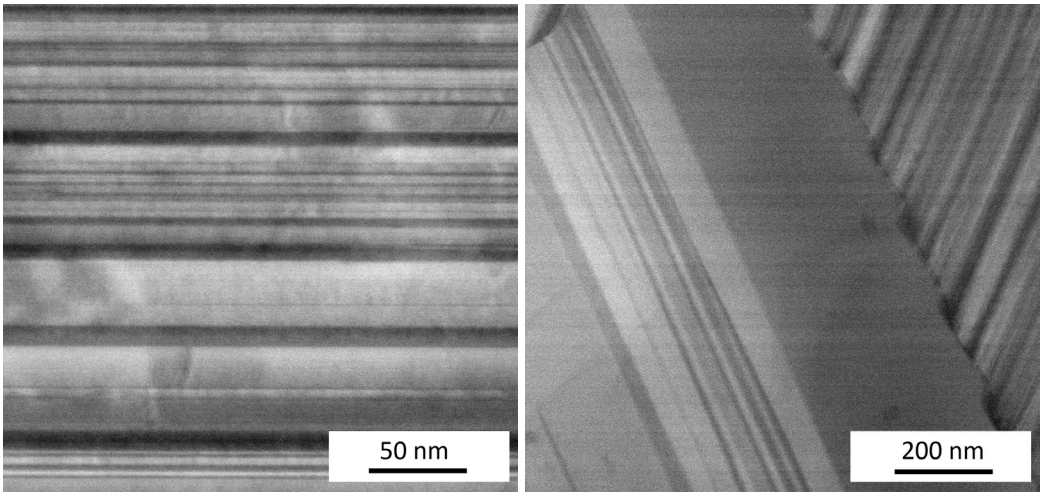

Fig. 8. TEM BF images from a specimen showing the wide variation in lamellar spacing and orientation, variation even present when these parameters are considered only for one phase.

TEM–BF images also showed that actual lamellar spacing can cover a wide size range, as can be observed in Fig. 8. Different contrasts are given by atomic arrangement, i.e., phase as well as phase orientation.

4 Conclusions

The results presented herein highlight the microstructural outcomes of a γ-TiAl material processed via Powder Metallurgy (PM). The material demonstrated an absence of porosity and exhibited a near gamma (NG) microstructure. Through the application of three distinct thermal treatments—HT1, HT2, and HT3—it was achieved the formation of DP microstructures in HT1 and NFL structures in HT2 and HT3.

Various microstructural parameters, such as the presence of γ grains, lamellar colonies, colony size, and actual lamellar spacing, were found to be strongly dependent on the cooling rate and stabilization temperature. Notably, some specimens from HT2 underwent globulization. Microcracks were consistently observed across all initial microstructures, with a more prevalent detection in NFL cases, where there was almost a complete presence of γ grains and γ contrast lamellae.

The assessment of lamellar spacing revealed a wide range of actual spacings, dependent on the measurement technique employed. This necessitated the use of high magnifications through SEM and TEM, which produced varying contrasts based on the crystallographic orientation and phase involved. Future investigations will aim to further elucidate the influence of these parameters on the microstructure and mechanical properties of γ-TiAl alloys, particularly focusing on optimizing processing conditions to minimize defects and enhance material performance.

Acknowledgments

This work is part of a master's thesis carried out at Universidad Carlos III of Madrid in collaboration with IMDEA Materials Institute. The authors are grateful to Ms. Amalia San Roman of IMDEA Materials, Madrid, Spain, for her technical assistance with the metallographic aspects of the work. The authors also acknowledge Dr. Manuel Avella (IMDEA Materials Institute) for his technical assistance with SEM and TEM characterization.

References

[1] D. G. Morris and M. A. Muñoz-Morris. Intermetallics: Past, present and future. *Revista de Metalurgia (Madrid)*, SPEC. VOL.(c):498–501, 2005.

[2] K. Kothari, R. Radhakrishnan, and N. M. Wereley. Advances in gamma titanium aluminides and their manufacturing techniques. *Progress in Aerospace Sciences*, 55:1–16, 2012.

[3] A. Lasalmonie. Intermetallics: Why is it so difficult to introduce them in gas turbine engines? *Intermetallics*, 14(10-11):1123–1129, 2006.

[4] F. Appel, J. D. H. Paul, and M. Oehring. *Gamma Titanium Aluminide Alloys: Science and Technology*. Wiley-VCH Verlag GmbH & Co. KGaA, Weinheim, Germany, 2011.

[5] H. Clemens and H. Kestler. Processing and applications of intermetallic γ-TiAl-based alloys. *Advanced Engineering Materials*, 2(9):551–570, 2000.

[6] R. M. Moreno. *In situ analysis of the high temperature deformation and fracture mechanisms*. PhD thesis, University Carlos III of Madrid, May 2014.

[7] B. P. Bewlay, S. Nag, A. Suzuki, and M. J. Weimer. TiAl alloys in commercial aircraft engines. *Materials at High Temperatures*, 33(4-5):549–559, 2016.

[8] H. Clemens and S. Mayer. Intermetallic titanium aluminides in aerospace applications – processing, microstructure and properties. *Materials at High Temperatures*, 33(4-5):560–570, 2016.

[9] B. Liu and Y. Liu. *Powder metallurgy titanium aluminide alloys*. Elsevier Inc., 2015.

[10] C. Leyens and M. Peters. *Titanium and titanium alloys: Fundamentals and applications*. Wiley-VCH, 2003.

[11] U. Habel and B. J. McTernan. HIP temperature and properties of a gas-atomized γ-titanium aluminide alloy. *Intermetallics*, 12(1):63–68, 2004.

[12] G. Cao, L. Fu, J. Lin, Y. Zhang, and C. Chen. The relationships of microstructure and properties of a fully lamellar TiAl alloy. *Intermetallics*, 8(5-6):647–653, 2000.

[13] R. T. Zheng, G. A. Cheng, G. X. Cao X. J. Li, Y. G. Zhang L. F. Fu, and C. Q. Chen. The relationship between fracture toughness and microstructure of fully lamellar TiAl alloy. *Journal of Materials Science*, 42(4):1251–1260, 2007.

[14] R. Gerling, H. Clemens, and F. P. Schimansky. Powder metallurgical processing of intermetallic gamma titanium aluminides. *Advanced Engineering Materials*, 6(1-2):23–38, 2004.

[15] D. Y. Seo, L. Zhao, and J. Beddoes. Microstructural evolution during heat treatments in Ti-45 and 47Al-2Nb-2Mn + 0.8 vol% TiB_2 XDTM alloys. *Materials Science and Engineering A*, 329-331:130–140, 2002.

[16] M. Su, Z. Lang, L. Zheng, J. Yan, K. Guan, and H. Zhang. Effect of heat treatment on microstructures and mechanical properties in a full lamellar TiAl alloy. *Materials Science and Engineering A*, 15(3):455–460, 2012.

[17] T. Novoselova, S. Malinov, and W. Sha. Experimental study of the effects of heat treatment on microstructure and grain size of a gamma TiAl alloy. *Intermetallics*, 11(5):491–499, 2003.

[18] G. Wegmann, R. Gerling, and F. Peter Schimansky. Temperature induced porosity in hot isostatically pressed gamma titanium aluminide alloy powders. *Acta Materialia*, 51(3): 741–752, 2003.

[19] Z. Zhang, Q. Sun, C. Li, and W. Zhao. Theoretical calculation of the strain-hardening exponent and strength coefficient of intermetallic gamma titanium aluminide alloys. *Journal of Materials Engineering and Performance*, 15(1):22–26, 2006.

[20] K. Young-Won. Intermetallic alloys based on gamma titanium aluminide. *JOM*, 41(7): 24–30, 1989.

The publication of this article was funded by the European Organization For Nuclear Research 10.13039/100012470